Controlling surface statistical properties using bias voltage: Atomic force microscopy and stochastic analysis

P. Sangpour,[1] G. R. Jafari,[1] O. Akhavan,[1] A. Z. Moshfegh,[1] and M. Reza Rahimi Tabar[1,2]

[1]*Department of Physics, Sharif University of Technology, P.O. Box 11365-9161, Tehran, Iran*
[2]*CNRS UMR 6529, Observatoire de la Côte d'Azur, BP 4229, 06304 Nice Cedex 4, France*

The effect of bias voltages on the statistical properties of rough surfaces has been studied using atomic force microscopy technique and its stochastic analysis. We have characterized the complexity of the height fluctuation of a rough surface by the stochastic parameters such as roughness exponent, level crossing, and drift and diffusion coefficients as a function of the applied bias voltage. It is shown that these statistical as well as microstructural parameters can also explain the macroscopic property of a surface. Furthermore, the tip convolution effect on the stochastic parameters has been examined.

I. INTRODUCTION

As device dimensions continue to shrink into the deep submicron size regime, there will be increasing attention for understanding the thin-film growth mechanism and the kinetics of growing rough surfaces in various deposition methods. To perform a quantitative study on surfaces roughness, analytical and numerical treatments of simple growth models propose, quite generally, the height fluctuations have a self-similar character and their average correlations exhibit a dynamic scaling form.[1–6] In these models, roughness of a surface is a smooth function of the sample size and growth time (or thickness) of films. In addition, other statistical quantities such as the average frequency of positive slope level crossing, the probability density function (PDF), as well as drift and diffusion coefficients provide further complete analysis on roughness of a surface. Very recently, it has been shown that, by using these statistical variables in the Langevin equation, regeneration of rough surfaces with the same statistical properties of a nanoscopic imaging is possible.[7]

In practice, one of the effective ways to modify roughness of surfaces is applying a negative bias voltage during deposition of thin films,[8] while their sample size and thickness are constant. In bias sputtering, electric fields near the substrate are modified to vary the flux and energy of incident charged species. This is achieved by applying either a negative DC or RF bias to the substrate. Due to charge exchange processes in the anode dark space, very few discharge ions strike the substrate with full bias voltage. Rather a broad low energy distribution of ions bombard the growing films.

Generally, bias sputtering modifies film properties such as surface morphology, resistivity, stress, density, adhesion, and so on through roughness improvement of the surface, elimination of interfacial voids and subsurface porosity, creation of a finer and more isotropic grain morphology, and the elimination of columnar grains.[8]

In this work, the effect of bias voltage on the statistical properties of a surface, i.e., the roughness exponent, the level crossing, the probability density function, as well as the drift and diffusion coefficients has been studied. In this regard, we have analyzed the surface of Co(3 nm)/NiO(30 nm)/Si(100) structure [as a base structure in the magnetic multilayers, e.g., spin valves operated using giant magnetoresistance (GMR) effect[9,10]] fabricated by bias sputtering method at different bias voltages. The behavior of statistical characterizations obtained by nanostructural analysis has been also compared with behavior of sheet resistance measurement of the films deposited at the different bias voltages, as a macroscopic analysis.

II. EXPERIMENT

The substrates used for this experiment were *n*-type Si(100) wafers with resistivity of about 5–8 Ω cm and the dimension of 5×11 mm^2. After a standard RCA cleaning procedure and a short time dip in a diluted HF solution, the wafers were loaded into a vacuum chamber. The chamber was evacuated to a base pressure of about 4×10^{-7} Torr. To deposit nickel oxide thin film, first high purity NiO powder was pressed and baked overnight at 1400 °C in an atmospheric oven yielded a green solid disk suitable for thermal evaporation. Before each NiO deposition, a preevaporation was done for about 5 minutes. Then a 30 nm thick NiO layer was deposited on the Si substrate with applied power of about 350 watts resulted in a deposition rate of 0.03 nm/s at a pressure of 2×10^{-6} Torr. After that, without breaking the vacuum, a thin Co layer of 3 nm was deposited on the NiO surface by using DC sputtering technique. During the deposition, a dynamic flow of ultrahigh purity Ar gas with pressure of 70 mTorr was used for sputtering discharge. The discharge power to grow Co layers was considered around 40 watts that resulted in a deposition rate of about 0.01 nm/s. The thickness of the deposited films was measured by styles technique, and controlled *in situ* by a quartz crystal oscillator located near the substrate. The distance between the target (50 mm in diameter) and substrate was 70 mm. Before each deposition, a pre-sputtering was also performed for about 10 minutes. The deposition of Co layers was done at various negative bias voltages ranging from zero to −80 V at the same sputtering conditions. The schematic details about the way of exerting the bias voltage to the Si substrate can be found in Ref. 11.

155423-1

In order to analyze the deposited samples, we have used atomic force microscopy (AFM) on contact mode to study the surface topography of the Co layer. The surface topography of the films was investigated using Park Scientific Instruments (model Autoprobe CP). The images were collected in a constant force mode and digitized into 256×256 pixels with scanning frequency of 0.6 Hz. The cantilever of 0.05 N m^{-1} spring constant with a commercial standard pyramidal Si_3N_4 tip with an aspect ratio of about 0.9 was used. A variety of scans, each with size L, were recorded at random locations on the Co film surface. The electrical property of the deposited films was examined by four-point probe sheet resistance (R_s) measurement at room temperature.

III. STATISTICAL QUANTITIES

A. Roughness exponents

It is known that to derive a quantitative information of a surface morphology one may consider a sample of size L and define the mean height of growing film $\bar{h}$ and its roughness w by the following expressions[12]:

$$\bar{h}(L,t,\lambda) = \frac{1}{L} \int_{-L/2}^{L/2} h(x,t,\lambda) dx \qquad (1)$$

and

$$w(L,t,\lambda) = (\langle (h - \bar{h})^2 \rangle)^{1/2}, \qquad (2)$$

where t is proportional to deposition time and $\langle \cdots \rangle$ denotes an averaging over different samples, respectively. Moreover, we have introduced λ as an external factor which can apply to control the surface roughness of thin films. In this work, $\lambda \equiv V/V_{opt}$ is defined where V and V_{opt} are the applied and the optimum bias voltages, so that at $\lambda = 1$ the surface shows its optimal properties. For simplicity, we assume that $\bar{h} = 0$, without losing the generality of the subject. Starting from a flat interface (one of the possible initial conditions), we conjecture that a scaling of space by factor b and of time by factor b^z (z is the dynamical scaling exponent), rescales the roughness w by factor b^χ as follows:

$$w(bL,b^z t,\lambda) = b^{\chi(\lambda)} w(L,t,\lambda), \qquad (3)$$

which implies that

$$w(L,t,\lambda) = L^{\chi(\lambda)} f(t/L^z,\lambda). \qquad (4)$$

If for large t and fixed L ($t/L^z \to \infty$) w saturate, then $f(x,\lambda) \to g(\lambda)$, as $x \to \infty$. However, for fixed large L and $t \ll L^z$, one expects that correlations of the height fluctuations are set up only within a distance $t^{1/z}$ and thus must be independent of L. This implies that for $x \ll 1$, $f(x) \sim x^\beta g'(\lambda)$ with $\beta = \chi/z$. Thus dynamic scaling postulates that

$$w(L,t,\lambda) = \begin{cases} t^{\beta(\lambda)} g(\lambda) \sim t^{\beta(\lambda)}, & t \ll L^z, \\ L^{\chi(\lambda)} g'(\lambda) \sim L^{\chi(\lambda)}, & t \gg L^z. \end{cases} \qquad (5)$$

The roughness exponent χ and the dynamic exponent z characterize the self-affine geometry of the surface and its dy-

namics, respectively. The dependence of the roughness w to the $\bar{h}$ or t shows that w has a fixed value for a given time.

The common procedure to measure the roughness exponent of a rough surface is use of a surface structure function depending on the length scale $\Delta x = r$ which is defined as

$$S(r) = \langle |h(x + r) - h(x)|^2 \rangle. \qquad (6)$$

It is equivalent to the statistics of height-height correlation function $C(r)$ for stationary surfaces, i.e., $S(r) = 2w^2(1 - C(r))$. The second order structure function $S(r)$ scales with r as r^{ξ_2} where $\chi = \xi_2/2$.[1]

B. The Markov nature of height fluctuations

We have examined whether the data of height fluctuations follow a Markov chain and, if so, determine the Markov length scale l_M. As is well known, a given process with a degree of randomness or stochasticity may have a finite or an infinite Markov length scale.[13–17] The Markov length scale is the minimum length interval over which the data can be considered as a Markov process. To determine the Markov length scale l_M, we note that a complete characterization of the statistical properties of random fluctuations of a quantity h in terms of a parameter x requires evaluation of the joint PDF, i.e., $P_N(h_1,x_1; \ldots ; h_N,x_N)$, for any arbitrary N. If the process is a Markov process (a process without memory), an important simplification arises. For this type of process, P_N can be generated by a product of the conditional probabilities $P(h_{i+1},x_{i+1}|h_i,x_i)$, for $i = 1, \ldots, N-1$. As a necessary condition for being a Markov process, the Chapman-Kolmogorov equation,

$$P(h_2,x_2|h_1,x_1) = \int d(h_i) P(h_2,x_2|h_i,x_i) P(h_i,x_i|h_1,x_1) \quad (7)$$

should hold for any value of x_i, in the interval $x_2 < x_i < x_1$.[15]

The simplest way to determine l_M for stationary or homogeneous data is the numerical calculation of the quantity, $S = |P(h_2,x_2|h_1,x_1) - \int dh_3 P(h_2,x_2|h_3,x_3) P(h_3,x_3|h_1,x_1)|$, for given h_1 and h_2, in terms of, for example, $x_3 - x_1$ and considering the possible errors in estimating S. Then, $l_M = x_3 - x_1$ for that value of $x_3 - x_1$ such that $S = 0$.

It is well known that the Chapman-Kolmogorov equation yields an evolution equation for the change of the distribution function $P(h,x)$ across the scales x. The Chapman-Kolmogorov equation formulated in differential form yields a master equation, which can take the form of a Fokker-Planck equation[15]:

$$\frac{d}{dr}P(h,x) = \left[-\frac{\partial}{\partial h}D^{(1)}(h,x) + \frac{\partial^2}{\partial h^2}D^{(2)}(h,x) \right] P(h,x). \quad (8)$$

The drift and diffusion coefficients $D^{(1)}(h,r)$, $D^{(2)}(h,r)$ can be estimated directly from the data and the moments $M^{(k)}$ of the conditional probability distributions:

$$D^{(k)}(h,x) = \frac{1}{k!} \lim_{r \to 0} M^{(k)},$$

$$M^{(k)} = \frac{1}{r} \int dh' (h' - h)^k P(h', x + r | h, x). \qquad (9)$$

The coefficients $D^{(k)}(h,x)$'s are known as Kramers-Moyal coefficients. According to Pawula's theorem,[15] the Kramers-Moyal expansion stops after the second term, provided that the fourth order coefficient $D^{(4)}(h,x)$ vanishes.[15] The fourth order coefficients $D^{(4)}$ in our analysis was found to be about $D^{(4)} \simeq 10^{-4} D^{(2)}$. In this approximation, we can ignore the coefficients $D^{(n)}$ for $n \geqslant 3$.

Now, analogous to Eq. (8), we can write a Fokker-Planck equation for the PDF of h that is equivalent to the following Langevin equation (using the Ito interpretation):[15]

$$\frac{d}{dx} h(x,\lambda) = D^{(1)}(h,x,\lambda) + \sqrt{D^{(2)}(h,x,\lambda)} f(x), \qquad (10)$$

where $f(x)$ is a random force, zero mean with Gaussian statistics, δ-correlated in x, i.e., $\langle f(x)f(x') \rangle = \delta(x - x')$. Furthermore, with this last expression, it becomes clear that we are able to separate the deterministic and the noisy components of the surface height fluctuations in terms of the coefficients $D^{(1)}$ and $D^{(2)}$.

C. The level crossing analysis

We have utilized the level crossing analysis in the context of surface growth processes, according to Refs. 18 and 19. In the level crossing analysis, we are interested in determining the average frequency (in spatial dimension) of observing of the definite value for height function $h = \alpha$ in the thin films grown at different bias voltages, $\nu_\alpha^+(\lambda)$. Then, the average number of visiting the height $h = \alpha$ with positive slope in a sample with size L will be $N_\alpha^+(\lambda) = \nu_\alpha^+(\lambda) L$. It can be shown that the ν_α^+ can be written in terms of the joint PDF of h and its gradient. Therefore, the quantity ν_α^+ carries the whole information of surface that lies in $P(h, h')$, where $h' = dh/dx$, from which we get the following result for the frequency parameter ν_α^+ in terms of the joint probability density function

$$\nu_\alpha^+ = \int_0^\infty p(\alpha, h') h' \, dh'. \qquad (11)$$

The quantity N_{tot}^+, which is defined as $N_{tot}^+ = \int_{-\infty}^{+\infty} \nu_\alpha^+ d\alpha$, will measure the total number of crossing the surface with positive slope. So, the N_{tot}^+ and square area of growing surface are in the same order. Concerning this, it can be utilized as another quantity to study further the roughness of a surface. It is expected that in the stationary state the N_{tot}^+ depends on bias voltages.

IV. RESULTS AND DISCUSSION

To study the effect of the bias voltage on the surface statistical characteristics, we have utilized AFM method for obtaining microstructural data from the Co layer deposited at the different bias voltages in the Co/NiO/Si(100) system. Figure 1 shows AFM micrographs of the Co layer deposited at various negative bias voltages of −20, −40, −60, and

−80 V, as compared with the unbiased samples.

For the unbiased very thin Co layer, Fig. 1(a) shows a columnar structure of the Co grains grown over the evaporated NiO underlying surface. However, Fig. 1(b) shows that by applying the negative bias voltage during the Co deposition, the columnar growth is eliminated. Moreover, Figs. 1(c) and 1(d) show that by increasing the bias voltage up to −60 V the grain size of the Co layer is increased, which means a more uniform and smoother surface is formed. But, for the bias voltage of −80 V, due to initiation of resputtering of the Co surface by the high energy ion bombardment, we have observed a nonuniform surface, even at the macroscale of the samples. Therefore, based on the AFM micrographs, the optimum surface morphology of the Co/NiO/Si(100) system was achieved at the bias voltage of −60 V for our experimental conditions.[20]

Now, by using the introduced statistical parameters in the last section, it is possible to obtain some quantitative information about the effect of bias voltage on surface topography of the Co/NiO/Si(100) system. Figure 2 presents the structure function $S(r)$ of the surface grown at the different bias voltages, using Eq. (6). The slope of each curve at the small scales yields the roughness exponent (χ) of the corresponding surface. Hence, it is seen that the surface grown at the optimum bias voltage (−60 V) shows a minimum roughness with $\chi = 0.60$, as compared with the other biased samples with $\chi = 0.75$, 0.70, and 0.64 for V = −20, −40, and −80 V, respectively. For the unbiased sample, we have obtained two roughness exponent values of 0.73 and 0.36, because of the nonisotropic structure of the surface [see Fig. 1(a)]. In any case, at large scales where the structure function is saturated, Fig. 2 shows the maximum and the minimum roughness values for the bias voltages of 0 and −60 V, respectively.

It is also possible to evaluate the grain size dependence to the applied bias voltage, using the correlation length achieved by the structure function represented in Fig. 2. For the unbiased sample, we have two correlation lengths of 30 and 120 nm due to the columnar structure of the grains. However, by applying the bias voltage, we can attribute just one correlation length to each curve showing elimination of the columnar structure in the biased samples. For the bias voltage of −20 V, the correlation length of r^* is found to be 56 nm. By increasing the value of the bias voltage to −40 and −60 V, we have measured $r^* = 76$ and 95 nm, respectively. However, at −80 V, due to initiation of the destructive effects of the high energy ions on the surface, the correlation length is reduced to 76 nm. Now, based on the above analysis, if we assume that $V_{opt} = -60$ V, then the roughness exponent and the correlation length can be expressed in terms of the λ as follows, respectively,

$$\chi(\lambda) = 0.61 + 0.16 \sin^2(2\pi\lambda/3.31 + 1.07), \qquad (12)$$

$$r^*(\lambda) = 53.50 + 40.23 \sin^2(2\pi\lambda/3.00 + 2.62)(\text{nm}), \qquad (13)$$

where for $\lambda = 0$ with the columnar structure, we have considered the average values.

To obtain the stochastic behavior of the surface, we need to measure the drift coefficient $D^{(1)}(h)$ and diffusion coeffi-
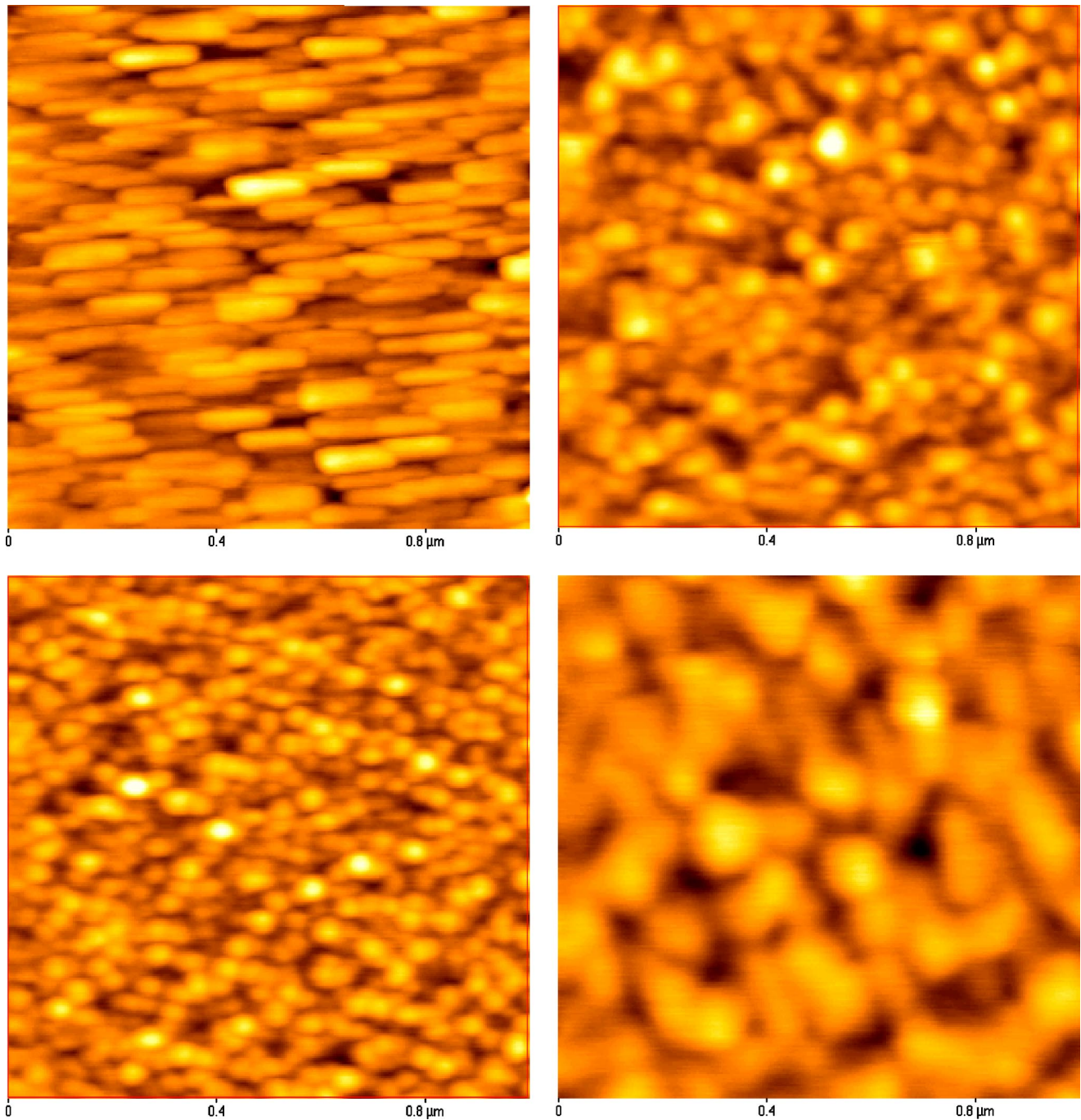
FIG. 1. (Color online) AFM surface images (all 1×1 μm^2) of Co(3 nm)/NiO(30 nm)/Si(100) thin films deposited at the bias voltages of (a) 0, (b) −20, (c) −40, and (d) −60 V (from top to bottom corresponding a to d, respectively).

cient $D^{(2)}(h)$ using Eq. (9). Figure 3 shows $D^{(1)}(h)$ for the surfaces at the different bias voltages. It can be seen that the drift coefficient shows a linear behavior for h as

$$D^{(1)}(h,\lambda) = -f^{(1)}(\lambda)h, \qquad (14)$$

where

$$f^{(1)}(\lambda) = [0.55 + 1.30 \sin^2(2\pi\lambda/3.50 + 1.40)] \times 10^{-4}. \qquad (15)$$

The minimum value of $f^{(1)}(\lambda)$ for the biased samples at $\lambda=1$ shows that the deterministic component of the height fluctuations for these samples is lower than the other biased and unbiased ones. Figure 4 presents $D^{(2)}(h)$ for the different bias voltages. At $\lambda=0$, the maximum value of diffusion has been obtained for any h, as compared with the other cases. By increasing the bias voltage, the value of $D^{(2)}$ is decreased, as can be seen for $\lambda=1/3$ and $2/3$. The minimum value of $D^{(2)}$, which is nearly independent of h, is achieved when $\lambda=1$. This shows that the noisy component of the surface
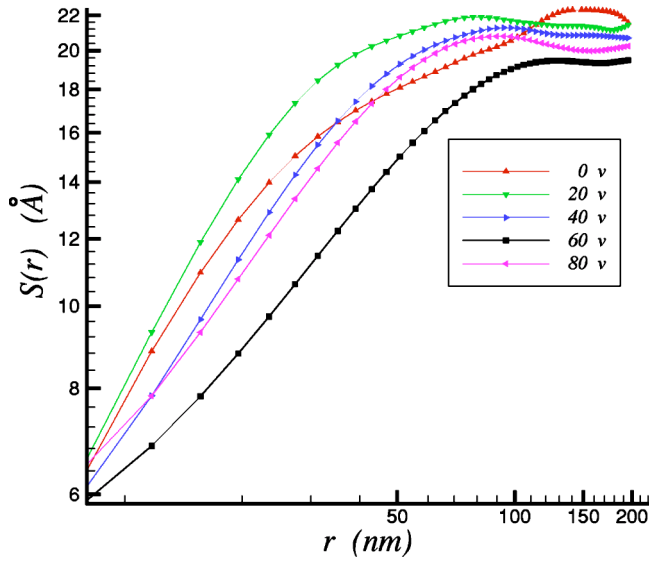
FIG. 2. (Color online) Log-log plot of structure function of the surface at different bias voltages.

height fluctuation at $\lambda=1$ is negligible as compared with the unbiased and the other biased samples. The behavior of $D^{(2)}$ at $\lambda=4/3$ becomes similar to its behavior at $\lambda=2/3$. It is seen that the diffusion coefficient $D^{(2)}$ is approximately a quadratic function of h. Using the data analysis, we have found that

$$D^{(2)}(h,\lambda) = f^{(2)}(\lambda)h^2, \tag{16}$$

where

$$f^{(2)}(\lambda) = [3.20 + 3.53 \sin^2(2\pi\lambda/3.33 + 1.34)] \times 10^{-6}. \tag{17}$$

Now, using the Langevin equation [Eq. (10)] and the measured drift and diffusion coefficients, we can conclude that
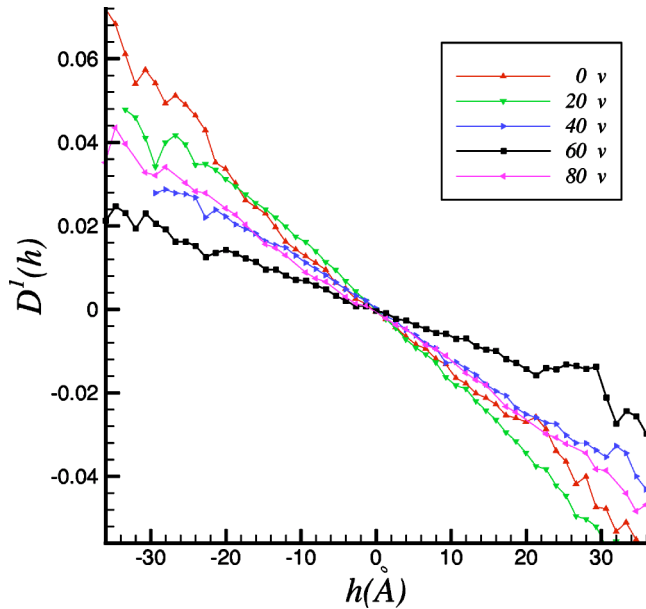
FIG. 3. (Color online) Drift coefficient of the surface at different bias voltages.
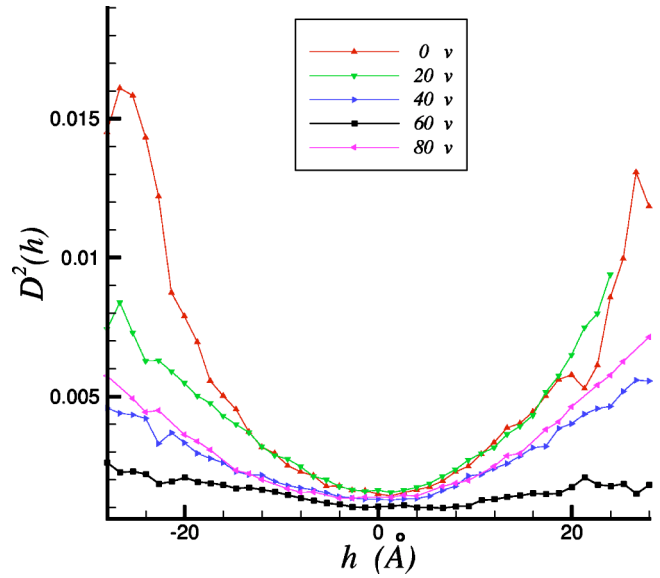

FIG. 4. (Color online) Diffusion coefficient of the surface at different bias voltages.

the height fluctuation has the minimum value at $\lambda=1$ which means a smoother surface at the optimum condition. Moreover, the obtained equations for the coefficients [Eqs. (14) and (16)] can be used to regenerate the rough surfaces the same as AFM images shown in Fig. 1.[7]

To complete the study, roughness of a surface can also be evaluated by the level crossing analysis, as another procedure. Figure 5 shows the observed average frequency ν_α^+ as a function of h for the different bias voltages. As λ is increased from 0 to 1, the value of ν_α^+ is decreased at any height. Once again, the optimum situation is observed for the bias voltage of -60 V, showing that the surface formed at $\lambda=1$ condition is a smoother surface with lower height fluctuations than the surface formed at the other conditions. It is seen that, at
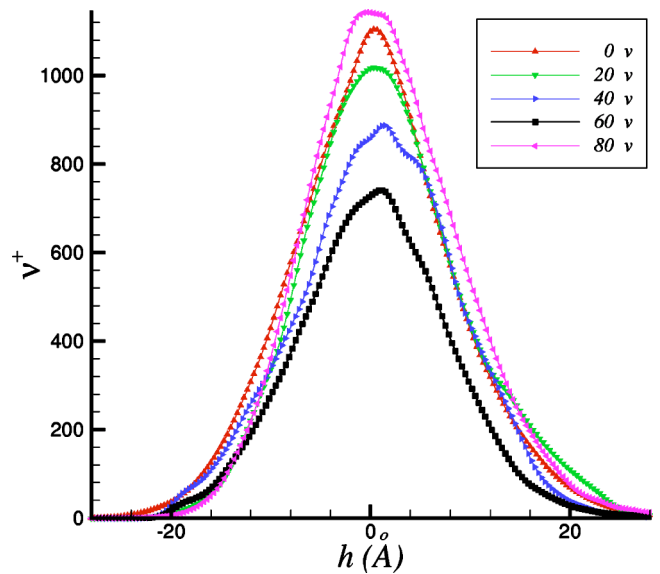

FIG. 5. (Color online) Level crossing of the surface at different bias voltages.
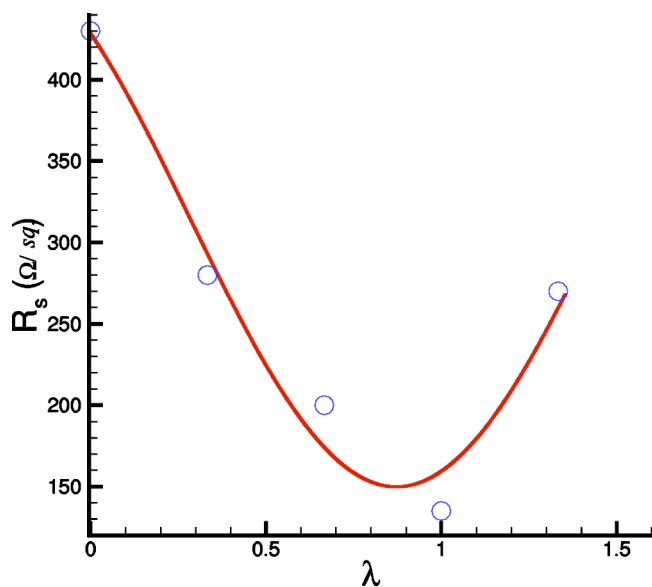
FIG. 6. (Color online) Sheet resistance measurement of the Co thin layer as a function of the applied bias voltage.
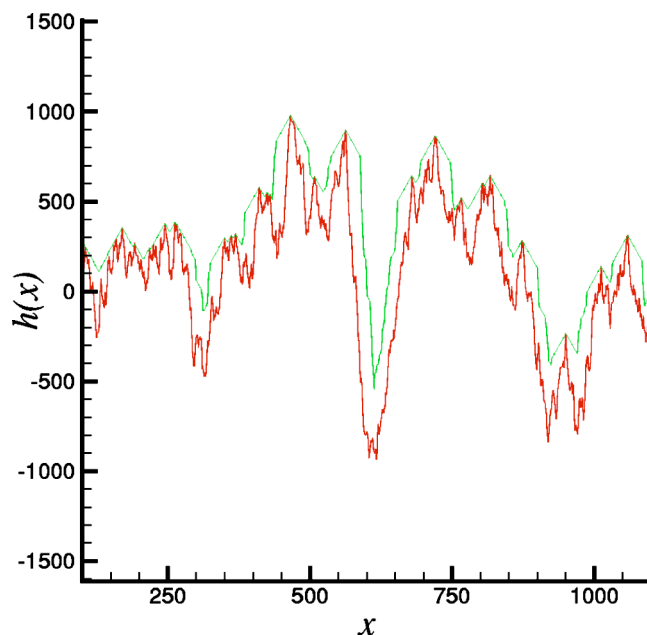

FIG. 7. (Color online) Height profile of a rough generated surface before dilation (real) and after dilation (tip) caused by a tip with the aspect ratio of 0.73.

$\lambda = 4/3$, the height fluctuation of the surface finds a maximum value, as compared with the other surfaces. The same as the roughness exponent and the correlation length behavior in terms of λ, the N_{tot}^{+} can be also expressed as

$$N_{tot}^{+}(\lambda) = [1.20 + 0.17 \sin^2(2\pi\lambda/3.52 + 1.40)]. \quad (18)$$

Since the system under investigation has a thin Co layer which is the only conductive layer, thus, it is obvious that lower height fluctuation corresponds to smaller electrical resistivity of the surface. Concerning this, we have measured sheet resistance of the Co surface grown at the different bias voltages, as shown in Fig. 6. For the bias voltage ranging from 0 to -60 V, the R_s value is reduced from 432 to 131 $\Omega/\square$. The minimum value of R_s is measured at the optimum condition of -60 V ($\lambda = 1$) which can be related to modified and smooth surface roughness. Elimination of interfacial voids, as well as porosities, and reduction of impurities in the Co layer. A similar behavior was also observed at $V_{opt} = -50$ V for Ta/Si(111) system.[21] By increasing the applied bias voltage to values greater than its optimum value, surface roughness is increased because of surface bombardment by high energy ions. This can be seen by the observed increase in the R_s value at the bias voltage of -80 V ($\lambda = 4/3$). It is easy to determine that the variation of R_s as a function of λ can be expressed as

$$R_s(\lambda) = [135.48 + 307.74 \sin^2(2\pi\lambda/3.93 + 1.77)]. \quad (19)$$

It behaves similar to the behavior of roughness characteristics of the surfaces. Therefore, we have shown that the roughness behavior explained by the statistical characterizations of the surface, which have been obtained by using microstructural analysis of AFM, can be related to the sheet resistance measurement of rough surfaces, as a macrostructural analysis.

V. THE TIP CONVOLUTION EFFECT

It is well known that images acquired with AFM are a convolution of tip and sample interaction. In fact, using scanning probe techniques for determining scaling parameters of a surface leads to an underestimate of the actual scaling dimension, due to the dilation of tip and surface. Concerning this, Aue and Hosson[22] showed that the underestimation of the scaling exponent depends on the shape and aspect ratio of the tip, the actual fractal dimension of the surface, and its lateral/vertical ratio. In general, they proved that the aspect ratio of the tip is the limiting factor in the imaging process.

Here we want to study the aspect ratio effect of the tip on the investigated stochastic parameters. To do this, using a computer simulation program, we have generated a rough surface by using a Brownian motion type algorithm[23] with roughness and its exponent of 10.00 nm and 0.67, respectively. We have assumed these roughness parameters in order to have some similarity between the generated surface and our analyzed surface by AFM. In the simulation program, the generated surface has been scanned using a sharp cone tip with an assumed aspect ratio of 0.73 that is also nearly similar to the applied tip in our AFM analysis with the aspect ratio of 0.9. Moreover, this assumption does not limit the generality of our discussion, because it is shown that the fractal behavior of a rough surface presents an independent tip aspect ratio behavior (saturated behavior) for the aspect ratios greater than about 0.4.[22]

Figure 7 shows a line profile of a generated surface that is dilated by a tip with the known aspect ratio. It is clearly seen that the scanned image (the image affected by the tip convolution) does not completely show the generated surface topography (real surface). Now it is possible to study the dependance of the examined surface stochastic parameters on
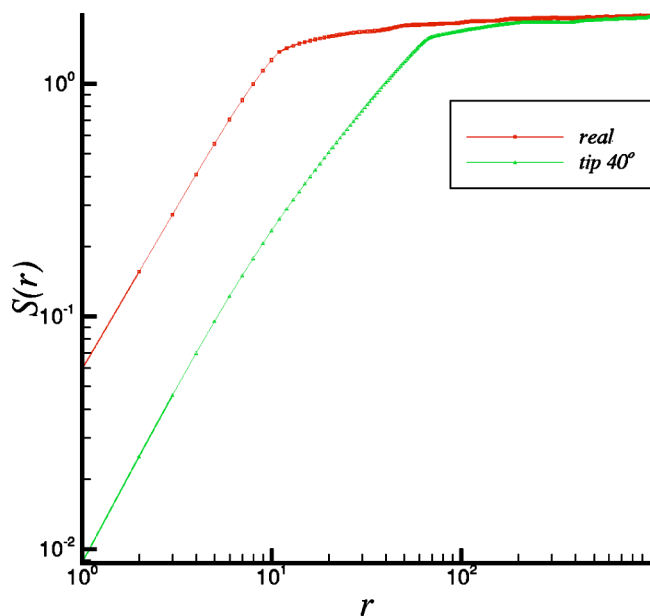
FIG. 8. (Color online) The one-dimensional structure function analysis, plotting $\log[S(r)]$ vs $\log(r)$ in which r is pixel position along the x axis. This results in the roughness values of 10 and 7.36 nm for the generated surface before dilation and after dilation using a tip with the aspect ratios of 0.73, respectively.

the geometrical characteristic of the tip, i.e., aspect ratio.

In this regard, Fig. 8 shows variation of the one-dimensional structure function of the generated rough surface due to the tip convolution effect. It can be seen that by increasing the aspect ratio the tip convolution results in obtaining a surface image with a decreased roughness. Since the aspect ratio of the applied AFM tip was around 0.9, so the measured roughness exponents at the different bias voltages might be corrected by a 1.07 factor. In other words, the relative change (the difference between the real and measured values comparing the real one) of the roughness exponent is about 7.2%. Moreover, Fig. 8 shows that the correlation length is increased by the tip convolution effect. It should be noted that, in our simulation, we have assumed that the apex of the tip is completely sharp (the tip radius is assumed to be zero). However, it is well known that the radius of the pyramidal tips is ~ 20 nm. Therefore, the real correlation lengths are even roughly 20 nm larger than the measured ones by the sharp tip.

The same tip convolution effect can be also presented for the drift and diffusion coefficients. Figure 9 presents the calculated drift coefficient for the generated surface and the scanned surface. One can see that the tip convolution results in decreasing of the drift coefficient, corresponding to decreasing of the surface roughness. This means that after dilation the correlation length will increase and hence the measured value for $f^{(1)}(\lambda)$ will be smaller than its value for the original surface. Therefore, the magnitude of slope of the drift coefficient must decrease after using the tip. For our generated surface, the measured value of the drift coefficient should be modified by a factor of around 2.

The variation of the diffusion coefficient of the generated rough surface due to the tip convolution effect has also been
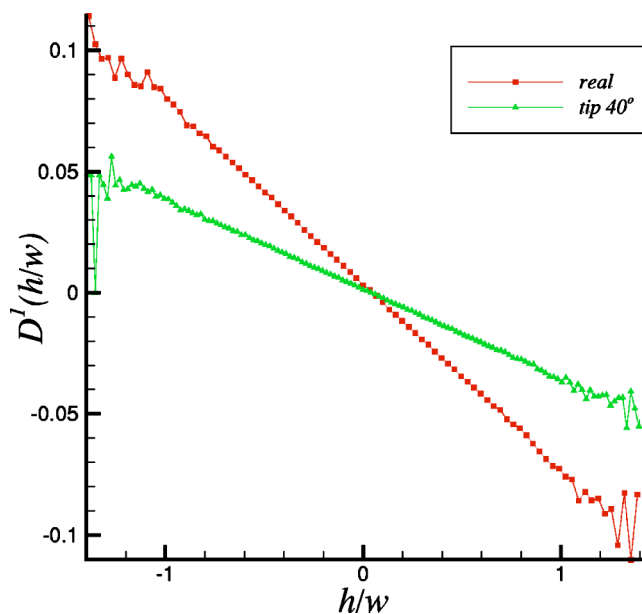

FIG. 9. (Color online) The calculated drift coefficient for the generated surface before dilation (real) and after dilation with a tip having aspect ratio of 0.73 (tip).

shown in Fig. 10. The reduction of the diffusion coefficient of the scanned surface as compared to its values for the generated surface, due to the tip convolution, can be easily seen. In fact, to compensate the tip effect on the diffusion coefficient, we should modify its measured values by a factor of about 4, for the assumed generated surface.

Finally, we remind that the total number of crossing the surface with positive slope (N_{tot}^{+}) has been defined as a parameter describing the rough surfaces. Hence, we have also studied the effect of the tip convolution on this parameter, as shown in Fig. 11. It is seen that N_{tot}^{+} decreased due to the tip convolution effect. For the assumed generated surface, we
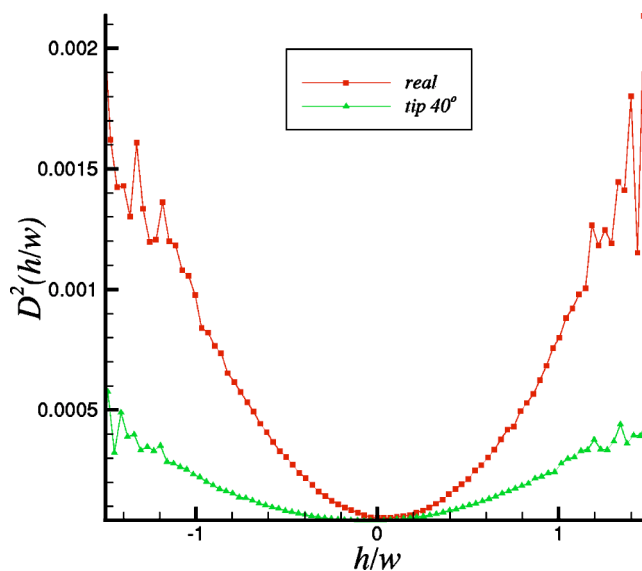

FIG. 10. (Color online) The calculated diffusion coefficient for the generated surface before dilation (real) and after dilation with a tip having aspect ratio of 0.73 (tip).
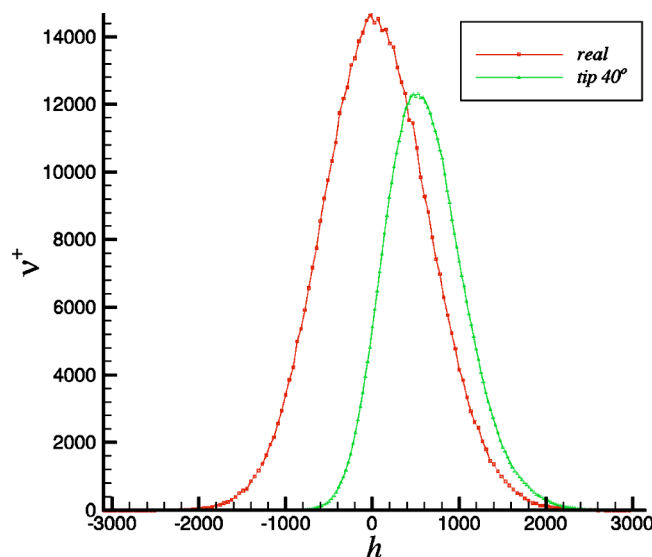
FIG. 11. (Color online) Level crossing analysis of the generated surface before dilation (real) and after dilation (tip).

have obtained that the N_{tot}^+ of the surface before dilation is about 1.7 times larger than its value after the dilation. In this figure, we have also shown the variation of the average height due to the tip effect.

One has to note that our generated surface is a pure two-dimensional one that presents no line-to-line interaction. So, for this simple model, differently shaped tips with the same aspect ratio yield the same results. Therefore, for the three-dimensional case one can expect to obtain a larger distortion of the surface due to stronger line-to-line interaction leading to an even larger underestimation of the studied stochastic parameters.

These analyses showed that, although the measured values of the surface parameters by AFM method are different from the real ones, the general behavior of these parameters as a function of the bias voltage is not affected by the tip convolution. Therefore, our general conclusions about the variation of the studied stochastic parameters by applying the bias voltage are intact.

VI. CONCLUSIONS

We have investigated the role of bias voltage, as an external parameter, to control the statistical properties of a rough surface. It is shown that at an optimum bias voltage ($\lambda=1$), the stochastic parameters describing a rough surface such as roughness exponent, level crossing, drift, and diffusion coefficient must be found in their minimum values as compared to an unbiased sample and the other biased samples. In fact, dependence of the height fluctuation of a rough surface on different kinds of external control parameters, such as bias voltage, temperature, pressure, and so on, can be expressed by AFM data which are analyzed using the surface stochastic parameters. In addition, this characterization enables us to regenerate the rough surfaces grown at different controlled conditions, with the same statistical properties in the considered scales, which can be useful in computer simulation of physical phenomena at surfaces and interfaces of, especially, very thin layers. It is also shown that these statistical and microstructural parameters can explain well the macroscopic properties of a surface, such as sheet resistance. Moreover, we have shown that the tip-sample interaction does not change the physical behavior of the stochastic parameters affected by the bias voltage.

[1] A. L. Barabasi and H. E. Stanley, *Fractal Concepts in Surface Growth* (Cambridge University Press, New York, 1995).

[2] T. Halpin-Healy and Y. C. Zhang, Phys. Rep. **254**, 218 (1995); J. Krug, Adv. Phys. **46**, 139 (1997).

[3] J. Krug and H. Spohn, *Solids Far From Equilibrium Growth, Morphology and Defects*, edited by C. Godreche (Cambridge University Press, New York, 1990).

[4] P. Meakin, *Fractals, Scaling and Growth Far From Equilibrium* (Cambridge University Press, Cambridge, England, 1998).

[5] M. Kardar, Physica A **281**, 295 (2000).

[6] A. A. Masoudi, F. Shahbazi, J. Davoudi, and M. Reza Rahimi Tabar, Phys. Rev. E **65**, 026132 (2002).

[7] G. R. Jafari, S. M. Fazeli, F. Ghasemi, S. M. Vaez Allaei, M. Reza Rahimi Tabar, A. Irajizad, and G. Kavei, Phys. Rev. Lett. **91**, 226101 (2003).

[8] M. Ohring, *Materials Science of Thin Films: Deposition and Structure* (Academic Press, New York, 2002).

[9] W. F. Egelhoff, Jr., P. J. Chen, C. J. Powell, M. D. Stiles, R. D. McMichael, C. L. Lin, J. M. Sivertsen, J. H. Judy, K. Takano, A. E. Berkowitz, T. C. Anthony, and J. A. Brug, J. Appl. Phys. **79**, 5277 (1996).

[10] B. Dai, J. N. Coi, and W. Lai, J. Magn. Magn. Mater. **27**, 19 (2003).

[11] A. Z. Moshfegh and O. Akhavan, J. Phys. D **34**, 2103 (2001).

[12] M. Marsilli, A. Maritan, F. Toigoend, and J. R. Banavar, Rev. Mod. Phys. **68**, 963 (1996).

[13] M. Waechter, F. Riess, Th. Schimmel, U. Wendt, and J. Peinke, Eur. Phys. J. B **41**, 259 (2004).

[14] J. Peinke, M. Reza Rahimi Tabar, M. Sahimi, and F. Ghasemi, cond-mat/0411529.

[15] H. Risken, *The Fokker-Planck Equation* (Springer, Berlin, 1984).

[16] J. Davoudi and M. Reza Rahimi Tabar, Phys. Rev. Lett. **82**, 1680 (1999).

[17] A. Irajizad, G. Kavei, M. Reza Rahimi Tabar, and S. M. Vaez Allaei, J. Phys.: Condens. Matter **15**, 1889 (2003).

[18] S. N. Majumdar and A. J. Bray, Phys. Rev. Lett. **86**, 3700 (2001).

[19] F. Shahbazi, S. Sobhanian, M. Reza Rahimi Tabar, S. Khorram, G. R. Frootan, and H. Zahed, J. Phys. A **36**, 2517 (2003).

[20] A. Z. Moshfegh and P. Sangpour, Phys. Status Solidi C **1**, 1744 (2004).

[21] A. Z. Moshfegh and O. Akhavan, Thin Solid Films **370**, 10 (2000).

[22] J. Aue and J. Th. M. De Hosson, Appl. Phys. Lett. **71**, 1347 (1997).

[23] H. Peitgen and D. Saupe, *The Science of Fractal Images* (Springer, Berlin, 1988).